AERODYNAMIC INTERACTIONS BETWEEN A 1/6-SCALE HELICOPTER ROTOR AND A BODY OF REVOLUTION

Mark D. Betzina
NASA Ames Research Center
Moffett Field, California

Patrick Shinoda
Aeromechanics Laboratory, U.S. Army Research and Technology Laboratories
NASA Ames Research Center
Moffett Field, California

Abstract

A wind-tunnel investigation was conducted in which independent, steady-state aerodynamic forces and moments were measured on a 2.24-m-diam, two-bladed helicopter rotor and a body of revolution. The objective was to determine the interaction of the body on the rotor performance and the effect of the rotor on the body aerodynamics for variations in velocity, thrust, tip-path-plane angle of attack, body angle of attack, rotor/body position, and body nose geometry. Results show that a body of revolution near the rotor can produce significant favorable or unfavorable effects on rotor performance, depending on the operating condition. Body longitudinal aerodynamic characteristics are significantly modified by the presence of an operating rotor and hub.

Nomenclature

A	rotor-disk area, m^2
b	number of rotor blades
c	rotor-blade chord, m
C_D	body wind-axis drag coefficient, D_B/qS_B
C_L	body wind-axis lift coefficient, L_B/qS_B
C_{L_R}	rotor wind-axis lift coefficient, $L_R/\rho(\Omega R)^2 A$
C_m	body wind-axis pitching moment coefficient $M_B/qS_B d$
d	maximum body diameter, m
D_B	body wind-axis drag, N
L_B	body wind-axis lift, N
$(L/D)_R$	rotor lift-to-drag ratio, $L_R/(P/V-PF)$
L_R	rotor wind-axis lift, N
M_B	body wind-axis pitching moment, N-m
P	rotor shaft power, W
PF	rotor propulsive force (negative wind-axis drag), N
q	free-stream dynamic pressure, Pa
R	rotor radius, m
S_B	body maximum cross-sectional area, m^2
T	rotor thrust (tip-path-plane axis), N
T'	corrected rotor thrust (tip-path-plane axis), $T(\rho_o/\rho)$, N
V	free-stream velocity, m/sec
X	longitudinal distance from hub center to body nose leading edge, m
Z	vertical distance from hub center to body surface, m
α_B	body geometric angle of attack, deg
α_{BC}	body angle of attack corrected for wall effect, $\alpha_B + \Delta\alpha$, deg
α_{TPP}	rotor geometric tip-path-plane angle of attack, deg
$\Delta\alpha$	wall correction to angle of attack, deg
μ	advance ratio, $V/\Omega R$
ρ	free-stream air density, kg/m^3
ρ_o	air density at standard conditions, kg/m^3
σ	rotor solidity, $bc/\pi R$
Ω	rotor rotational speed, rad/sec

Introduction

The aerodynamic flow field around an operating helicopter rotor is extremely complex. Current analytical techniques permit fair success in predicting the flow field around an isolated rotor or an isolated fuselage. However, the flow field around a real helicopter is influenced not only by the rotor, fuselage, tail, tail rotor, and engines, but also by the mutual interactions between these components.[1] Therefore, the aerodynamic characteristics are dependent on the entire helicopter system.

It has been shown that configuration parameters, such as rotor/fuselage separation, can affect the aerodynamic interactions in a manner which produces significant changes in performance, loads, and vibration. Reference 2 describes interactional aerodynamics problems that occurred during the YUH-61A UTTAS development program. The rotor height was subsequently raised during this program to alleviate some of these problems. Very little is understood about the detailed phenomena responsible for these interactions. Although prediction of the flow fields may be the ultimate

goal of helicopter designers, their effects on performance, loads, and vibration are of more immediate concern. Current analytical techniques fail to successfully predict the details of these complex flow fields, thereby providing inadequate estimations of total helicopter performance.

Much of the previous work on this subject has concentrated on the dynamic interactions affecting blade loads and fuselage vibration.[2] Although the dynamic effects are certainly a major concern, this investigation addresses only the steady-state aerodynamic interactions between rotor and body. References 3 through 5 describe investigations in which time-averaged fuselage surface pressures were measured for various configurations of rotors and bodies. Some success has been achieved in analytically predicting time-averaged surface pressures at an advance ratio of 0.05.[3]

Wind-tunnel tests of full-scale helicopter rotors have typically used a body of revolution to enclose the drive motors and transmission. Aerodynamic characteristics of the body of revolution without the rotor blades have simply been subtracted from the overall forces and moments to determine rotor performance. This approach ignores the mutual aerodynamic interactions between the rotor and body, and produces rotor performance in the presence of the body rather than isolated rotor performance.

The objective of this investigation was to obtain quantitative measurements of the steady-state aerodynamic interactions for a simplified helicopter system consisting of a rotor and body of revolution. The effect of the body on the rotor performance will be evaluated by comparing isolated rotor performance (without body) with rotor performance in the presence of the body. The effect of the rotor on the body aerodynamic characteristics will be evaluated by determining body lift, drag, and pitching-moment characteristics as a function of rotor-disk loading and operating condition. These data will provide: 1) a data base for correlation with and improvement of analytical techniques, 2) qualitative information about the trends of these interactions at full scale, and 3) some insight into the aerodynamic mechanisms that cause them.

Model Description

A simplified helicopter system, consisting of a teetering, two-bladed rotor and a body of revolution, was used for this investigation. The 2.235-m-diam rotor blades were aerodynamically scaled to 1/6-scale AH-1G Cobra blades. The blades were not scaled dynamicly, and had a relatively high stiffness compared with that of full-scale blades. The characteristics of the rotor are shown in Table 1. The hub, which was not scaled, had a diameter equal to 14% of the rotor diameter. The body for the baseline configuration was a 1/6-scale model of the rotor test apparatus (RTA), a body of revolution used for testing full-scale rotors in the Ames 40- by 80-Foot Wind Tunnel. The model did not include the strut attachment fairings and hub cutout which exist on the RTA. The model dimensions are shown in Fig. 1. The full-scale RTA is shown in the Ames 40- by 80-Foot Wind Tunnel in Fig. 2.

The rotor and body were installed in the Ames 7- by 10-Foot Wind Tunnel in an inverted position, that is, the rotor was installed below the body with the rotor producing downward thrust. The model installation is shown in Fig. 3. The rotor was installed on a test rig that was mounted on the wind-tunnel balance system. The rotor drive shaft housing was shielded from the wind by a fairing supported by the wind-tunnel floor. The body was mounted on a single strut supported by the wind-tunnel ceiling. There was no physical connection between the body and the rotor system; the normal rotor shaft between the fuselage and hub was not simulated. For the baseline configuration, the location of the body relative to the hub was scaled to the full-scale RTA design position. The baseline geometry is shown in Fig. 1. For the 2.235-m-diam rotor used, this resulted in a vertical separation of 8% of the rotor radius. The longitudinal location of the leading edge of the body nose, for the baseline configuration, was at 44.7% of the rotor radius. The body nose geometry was varied by installing a modified nose (shown in Fig. 1) which provided more upwash into the rotor, more closely simulating a typical helicopter cabin. This nose was also tested in an inverted position, reducing the upwash into the rotor. Steady-state forces and moments on the rotor were measured by the wind-tunnel balance system. The body forces and moments were measured by a six-component internal strain-gage balance.

Test Procedure

Data were obtained for the isolated rotor, isolated body, and combined rotor/body configurations at free-stream velocities up to 62 m/sec (120 knots). The rotor tip-path-plane orientation was determined from rotor flapping measurements. Tip-path-plane orientation was held constant, using cyclic pitch control, while thrust was varied, using collective pitch control. This procedure was used to obtain data for a sequence of thrust levels with various combinations of velocity, tip-path-plane angle of attack, body angle of attack, body nose shape, and rotor/body position. Ranges of the test parameters, which included trimmed rotor propulsive force for each advance ratio, are shown in Table 2. Angles of attack were defined with standard sign conventions, such that a free-stream velocity in the direction shown in Fig. 1 resulted in a positive body angle of attack and a positive tip-path-plane angle of attack. The rotor shaft angle remained constant while tip-path-plane angle varied. The position of the body was adjusted as body angle of attack varied, such that the hub location relative to the body remained constant. The rotor tip speed was held constant at 206 m/sec (675 ft/sec) throughout the test.

Data Reduction

Hub tares were removed from the measured rotor data to correct for the hub and controls that were exposed to the airstream. These tares were determined by obtaining force and moment data on the rotor rig with the rotor blades removed. This was done for each combination of body angle of attack, position, and nose geometry, as well as with the body removed, thereby accounting for the interference of the body on the hub (with blades off).

However, it was not possible to determine the effect of the rotor on these tares, since this would require separating the hub and control system forces from the rotor forces. Therefore, the computed rotor data includes the interference of the hub, controls, and support fairing on the rotor and the interference of the rotor on the hub and controls. These interferences are small related to the rotor forces and are consistent throughout the test so that the interaction of the body on the rotor is valid.

The effect of the body on the rotor performance was determined by plotting the rotor lift-to-drag ratio versus the rotor lift coefficient for various configurations. The rotor lift-to-drag ratio was calculated as follows:

$$(L/D)_R = \text{Lift} \; / \; (P/V - PF)$$

where PF is the measured propulsive force, P is rotor power, and V is free-stream velocity. The denominator in the above equation represents the sum of the induced and profile drag of the rotor. The lift-to-drag ratio was used since it is a measure of the rotor efficiency. As the lift-to-drag ratio increases, power required for a given flight condition decreases.

Body lift, drag, and pitching moment were defined as shown in Fig. 1. Body lift, drag, and pitching-moment coefficients were computed using the free-stream dynamic pressure and the maximum cross-sectional area of the body. The maximum diameter of the body was used for normalizing the pitching moment. The moment center was located on the longitudinal body axis, 0.50 m aft of the nose (approximately 30% body length), as indicated in Fig. 1. This corresponds to the longitudinal position of the rotor hub for the baseline configuration.

Wind-tunnel-wall corrections were used to determine the effective angle of attack of both the rotor and body; the reference system for the data was the corrected wind axis. The correction, obtained from the method in Ref. 6, was determined using the following equation:

$$\Delta\alpha = 1.084 \; L_R/q$$

where $\Delta\alpha$ is the angle-of-attack change in degrees, L_R is the rotor lift, and q is the free-stream dynamic pressure. The wind-tunnel walls produce an effective angle-of-attack change proportional to the rotor lift. The rotor and body orientation were not adjusted to maintain constant corrected angle of attack. Therefore, the tip-path-plane angle of attack and the body angle of attack indicated in Figs. 4 through 15 are the geometric angles in the wind tunnel.

Results and Discussion

Effect of Body on Rotor Performance

The performance of the rotor with the body removed is shown in Fig. 4 for the range of test conditions investigated. These data generally fall along a curve for each advance ratio. Rotors generally show a slight decrease of L/D with propulsive force increase (as tip-path-plane is tilted forward); this trend is not seen in Fig. 4 because of scatter in the data, caused mostly by the precision of the rotor power measurement obtained from the wind-tunnel balance system. The faired curve shown is the least squares, second-order polynomial curve fit of the data for each advance ratio. These curves are shown on Figs. 5-8 to indicate the isolated rotor performance.

Figure 5 shows the effect of the body on the rotor performance for the baseline configuration. Again, there is no clear trend of the influence of rotor tip-path-plane angle of attack. However, the influence of the body on rotor lift-to-drag ratio is clear. When the body angle of attack is 0°, the presence of the body produces an increase in rotor lift-to-drag ratio; hence, a favorable interference effect. When the body angle of attack is -4°, the body produces a favorable interference effect on the rotor performance at an advance ratio of 0.2, but an unfavorable effect at an advance ratio of 0.3. At a body angle of attack of -8°, the body produces an unfavorable interference effect on the rotor performance at advance ratios of 0.2 and 0.3. Data at intermediate angles of attack and advance ratios, which would help explain these results were not obtained; however, it appears that body angle of attack has a strong effect on the rotor performance at 0.2 and 0.3 advance ratios. The small effect at an advance ratio of 0.1 is consistent with the fact that any changes in free-stream flow direction caused by the body create very small angle-of-attack changes of the rotor blades, since the rotational velocity of the rotor is much greater than the free-stream velocity. This explanation would imply that the effect of the body would increase as advance ratio increases; however, Fig. 5 indicates that the free-stream velocity effect is overpowered by an interaction effect.

The effect of body angle of attack on the rotor performance is shown in Fig. 6 for the baseline configuration, with a rotor tip-path-plane angle of attack of -8°. A fairly consistent reduction in rotor lift-to-drag ratio is shown as body angle of attack varies from 0° to -8° for advance ratios of 0.2 and 0.3. This trend with body angle is consistent with the trends observed in Fig. 5, where the effect of the body on the rotor performance changes from favorable to unfavorable as body angle of attack varies from 0° to -8°.

Another parameter investigated was the separation between rotor and body. Data were obtained for separations of 8% and 10.2% of the rotor radius. A comparison of these results is shown in Fig. 7 for two configurations where the body and tip-path-plane angles of attack are equal. By maintaining the body angle of attack equal to the tip-path-plane angle of attack, the relationship between the body and rotor blades is identical. Therefore, the only difference between Figs. 7a and 7b is the free-stream flow direction. Figure 7a shows essentially no change in rotor performance caused by increasing the rotor/body separation at advance ratios of 0.1 and 0.3. However, at an advance ratio of 0.2, there is a reduction in lift-to-drag ratio as separation increases for intermediate thrust values. This is reasonable since the effect of the body is to increase the lift-to-drag ratio at this test condition. The greater separation reduces the effect of the body. In Fig. 7b, the rotor lift-to-drag ratio increases as separation increases for advance ratios of 0.2 and 0.3. Again, this is a reduction in the effect of the body. For an angle

of attack of -8° for both the body and tip-path-plane, and an advance ratio of 0.3, increasing the separation from 8% to 10.2% of the rotor radius reduces the effect of the body by about 50%; for an angle of attack of 4° there is no observable change. Therefore, the effect of separation is dependent on angle of attack.

Figure 8 shows the effect of rotor/body separation for a body angle of attack of 0°, and at advance ratios of 0.2 and 0.3. In this case, however, the tip-path-plane angle of attack is -4°. This places the rotor blades closer to the body on the forward part and farther from the body on the aft part when compared with the configuration in Fig. 7. Figure 8 indicates a much greater effect of separation than is shown in Fig. 7. In fact, the effect of the body on rotor lift-to-drag ratio changes from favorable to unfavorable by increasing the separation from 8% to 10.2% of the rotor radius. At a body angle of attack of 0°, there is a much larger flow disturbance near the upper portion of the nose than when the body is at a negative angle of attack. This, combined with the proximity of the rotor blades in this area owing to the forward tilt of the tip-path-plane, may be creating a particular flow such that there is a separation distance where the rotor lift-to-drag ratio is a minimum; as a result, rotor performance may be increased by either increasing or decreasing the rotor/body separation. Insufficient data were obtained during this investigation to determine if this is true. Data for a complete series of separation distances are required to answer this question.

The effect of moving the body forward relative to the rotor is also shown in Fig. 8. The body was moved forward by 9% of the rotor radius; this located the nose at 53.8% of the rotor radius. The vertical separation was maintained at 10.2% radius. As shown in Fig. 8, this produces a significant increase in rotor performance.

Figure 9 shows the effect of changes in body nose shape on rotor performance. The nose modification, shown in Fig. 1, was installed in both upright and inverted positions. The modified nose causes a significant reduction in rotor lift-to-drag ratio when compared with the baseline nose, particularly at an advance ratio of 0.3. However, reducing the upflow into the rotor by inverting the modified nose, appears to have very little effect. Part of the effect of the modified nose may be caused by the change in longitudinal nose position. However, Fig. 8 indicates an increase in rotor performance when the baseline nose is moved forward. The data for the modified nose were obtained only for a body angle of attack of 0°, but it appears that nose shape is an important parameter and that the interference effect of the nose depends on more than simply the upflow produced by the nose.

Effect of Rotor on Body

Figure 10 shows the longitudinal characteristics for the isolated body, the body in the presence of the rotating hub, and the body in the presence of the hub and rotor in the baseline configuration. The interaction of the hub on the body causes a large positive shift in lift and drag, and a negative shift in the pitching moment, as well as slope changes. The hub for this investigation is not scaled to a typical size for a helicopter hub, since the size is determined by the structural requirements. Therefore, this large hub effect is probably greater than the effect of a relatively smaller hub, which would exist at full-scale. Apparently, the hub wake creates a low-pressure region on the surface of the body behind the hub. This produces increased lift, negative pitching moment, and increased drag, possibly an induced drag. It is expected that this hub interaction is substantially modified when subjected to the rotor wake.

The total effect of the rotor and hub on the body is the sum of the rotor interaction and the modified interaction of the hub. The rotor effect on the body without the hub cannot be determined from these data, because there is no way of separating the direct rotor interaction from a modification of the hub's interaction. Because of this, Figs. 11 through 15 present trends of the body forces and moments with variations in the test parameters, but no attempt is made to make comparisons with isolated body characteristics.

Figure 11 shows the effect of varying rotor thrust on the body longitudinal characteristics for the baseline configuration and a free-stream velocity of 41.2 m/sec. Body lift, drag, and pitching-moment coefficients are plotted versus rotor-disk loading. The body-lift coefficient increases proportionally with thrust at about the same rate for all cases shown. The drag coefficient increases at low rotor thrust and the pitching-moment coefficient becomes less negative as rotor thrust increases at tip-path-plane angles of attack of -4° and -8°.

At a body angle of attack of -4°, the decrease in drag with increased disk loading at negative tip-path-plane angles is greater than at a body angle of attack of 0°; however, the trend with tip-path-plane angle is opposite. The slopes of the drag curves increase as tip-path-plane angle-of-attack increases negatively, but the slopes of the lift and pitching-moment curves, appear to be unchanged. These results cannot be explained as a simple angle-of-attack change caused by differences in the rotor wake velocity; the increased downward wake velocity, as thrust increases, would cause a negative angle-of-attack increment, decreasing the lift coefficient.

The wind-tunnel-wall effect produces an effective angle-of-attack increase as thrust increases. But, based on the lift curve slope shown in Fig. 10, the wall effect accounts for only a small portion of the increased lift shown in Fig. 11. A possible explanation for the observed lift trend is that the rotor wake interacts with the hub wake such that the lift on the aft portion of the body is increased. But this would produce a negative increment in pitching moment, a result opposite of the pitching moment trend shown. Another possible explanation for the lift trend is an increased upflow component near the forward portion of the body as thrust increases. This can be visualized as an upflow upstream of the lifting rotor disk, as if it were a circular wing. Detailed measurements of the flow characteristics are needed to define the specific phenomena that produce these interactions.

Figure 12 shows the ratios of body lift to rotor thrust and of drag to rotor thrust for a constant disk loading of 240 Pa (5 lb/ft^2). The ratios of body forces to rotor thrust are used to indicate the significance of the interactions. Various combinations of advance ratio, rotor tip-path-plane angle of attack, and body angle of attack are shown for the baseline configuration. Since the rotor tip speed is constant, the change in advance ratio is made by changing the free-stream velocity. The body lift and drag include the dynamic pressure effect, which increases the body forces as the advance ratio increases.

At an advance ratio of 0.3, with the tip-path-plane at an angle of attack of -8°, the body lift is 2.5% of the rotor thrust when the body angle-of-attack is 0°, and about 1.2% when the body angle of attack is -4°. The body lift decreases as the tip-path-plane angle is moved toward zero.

The data show a fairly linear variation of body lift with tip-path-plane angle. Since the total vehicle drag is typically much smaller than the rotor thrust, small changes in the drag ratio shown are more important in determining the power required, especially at high speeds. The drag of this body is much lower than the drag of a typical helicopter fuselage; it is also lower than the full-scale RTA. The body-drag results for body angles of attack of 0° and -4° are very similar. However, at an advance ratio of 0.2, tilting the tip-path-plane forward increases the drag when the body angle of attack is 0°, but has almost no effect when the body angle of attack is -4°. At an advance ratio of 0.3, the body drag is lowest when the tip-path-plane angle of attack is -4°.

Figure 13 shows the body lift, drag, and pitching-moment coefficients as functions of rotor-disk loading for various rotor/body positions. For the operating condition shown, increasing the rotor/body separation from 8% to 10.2% of the rotor radius decreases the body-lift coefficient and produces a positive shift in the body-pitching moment. The lift change is independent of disk loading, but the pitching-moment change appears to be greater at lower thrust levels. The drag change is relatively small. Moving the body forward relative to the rotor, however, causes a large increase in body drag coefficient. This is associated with a negative shift in pitching moment and lift coefficients that is independent of disk loading.

Figure 14 shows the effect of rotor/body separation for various combinations of advance ratios and body angles of attack at constant disk loading. The tip-path-plane angle of attack is -4°. In terms of percent of rotor thrust, the body-lift change is negligible; however, there are significant changes in body drag for most of the operating conditions. The body drag increases as the rotor/body separation is increased from 8% to 10.2% of the rotor radius. This change in body drag is greater for a body angle of attack of -4° than it is for 0°.

Figure 15 shows the effect of longitudinal position on body lift and drag for constant rotor-disk loading. Figures 12 and 14 indicate that the variation of body lift and drag with advance ratio is generally nonlinear; however, data for only two advance ratios were obtained for this configuration. The decrease in body lift caused by moving the body forward relative to the rotor is about 0.2% of the rotor thrust at advance ratios of 0.2 and 0.3. This lift decrease is associated with a drag increase of 0.6% of the rotor thrust at 0.2 advance ratio, but only a negligible increase at an advance ratio of 0.3

Since the measured body forces and moments include the interaction of the unscaled hub, as well as the rotor interaction, the magnitude of the data may not be representative of full-scale. It is also expected that Reynolds number is important in determining the magnitude of these interactions, since separated flow regions are involved. Therefore, extrapolating the magnitude of the body forces and moments to full-scale is not recommended. It is expected, however, that the trends observed in this investigation are similar to those at full-scale with an appropriately sized hub. Full-scale testing is required to verify this.

Conclusions

1. Rotor performance is significantly affected by the presence of a body of revolution near the rotor. This interaction can be either favorable or unfavorable, depending on the configuration and operating condition. Parameters with a strong influence on this interaction are advance ratio, body angle of attack, rotor/body separation, rotor/body longitudinal relationship, and body nose shape. Parameters with a weak influence on this interaction are rotor tip-path-plane angle of attack and rotor thrust.

2. The longitudinal aerodynamic characteristics of a body of revolution are significantly modified by the presence of an operating rotor and hub. The hub may be a major source of this interaction. Therefore, to determine the magnitude of the interaction, it is necessary to have a properly scaled hub. This may require full- or large-scale testing.

3. Rotor performance data, determined by testing full-scale rotors, generally include the rotor/body interaction effects. These effects may be significant even when a body of revolution is used (as is typically done in wind-tunnel testing). Full-scale measurements of these interactions are required to determine their magnitudes.

The following interaction effects of the rotor and hub on the body aerodynamic characteristics were observed:

1. Body lift increases proportionally with rotor thrust.

2. Body lift increases as the rotor tip-path-plane is tilted forward at constant thrust.

3. When the body and tip-path-plane are at negative angles of attack, body drag decreases and body pitching moment becomes less negative as rotor thrust increases.

4. The interaction is dependent on the body position relative to the rotor.

References

[1]Sheridan, P. F. and Smith, R. P., "Interactional Aerodynamics — A New Challenge to Helicopter Technology," Paper No. 79-59, 35th Annual Forum of the American Helicopter Society, Washington, D. C. May 1979.

[2]Sheridan, P. F., "Interactional Aerodynamics of the Single Rotor Helicopter Configuration," USARTL-TR-78-23, Sept. 1978.

[3]Freeman, Carl E. and Wilson, John C., "Rotor-Body Interference (ROBIN) — Analysis and Test," Paper No. 80-5, 36th Annual Forum of the American Helicopter Society, Washington, D. C., May 1980.

[4]Wilson, John C. and Mineck, Raymond, E., "Wind-Tunnel Investigation of Helicopter-Rotor Wake Effects on Three Helicopter Fuselage Models," NASA TM X-3185, 1975.

[5]Freeman, Carl E. and Mineck, Raymond E., "Fuselage Surface Pressure Measurements of a Helicopter Wind-Tunnel Model with a 3.15-Meter Diameter Single Rotor," NASA TM-80051, 1979.

[6]Pope, A. and Harper, J. J., Low-Speed Wind Tunnel Testing, John Wiley & Son, Inc., 1966.

Table 1. Rotor Geometry

Number of blades, b	2
Rotor radius, R	1.118 m
Blade chord, c	0.114 m
Rotor solidity, $bc/\pi R$	0.0651
Blade precone angle, a_o	1.33°
Blade twist (linear)	-10°
Blade taper ratio	1.0
Airfoil	modified NACA 0012
Flapping hinge undersling	0.0091 m
Blade lock number	3.44

Table 2. Test Parameters

Advance ratio, μ	0.1, 0.2, 0.3
Tip Mach number	0.6
Body angle of attack, α_B	0°, -4°, -8°
Tip-path-plane angle of attack, α_{TPP}	0°, -4°, -8°
Rotor-disk loading, T/A	110 to 340 Pa
Rotor/body separation, Z/R	0.080, 0.102
Rotor/body longitudinal position, X/R	0.447, 0.538

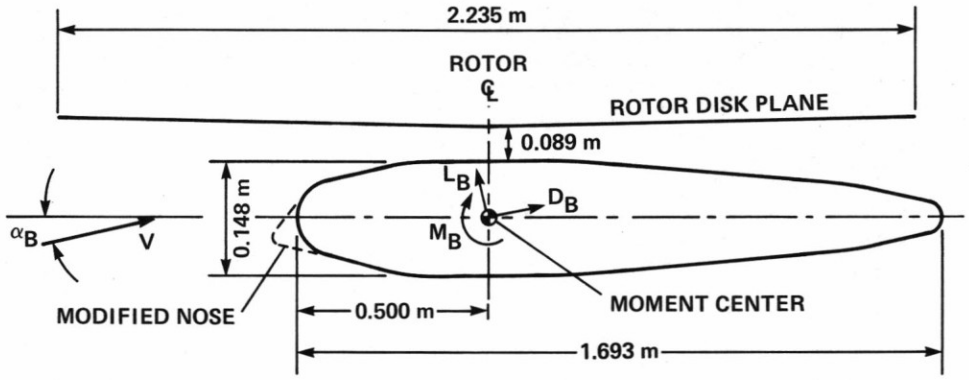

NOTE: POSITIVE BODY FORCES AND MOMENTS SHOWN

Figure 1. 1/6 — Scale RTA body of revolution shown with rotor in baseline position.

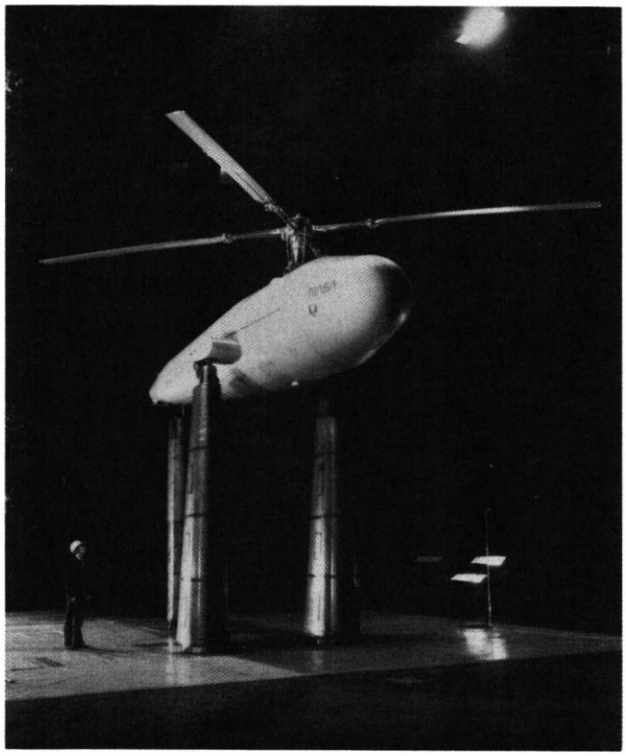

Figure 2. Full-scale rotor test apparatus in the Ames 40- By 80-Foot Wind Tunnel.

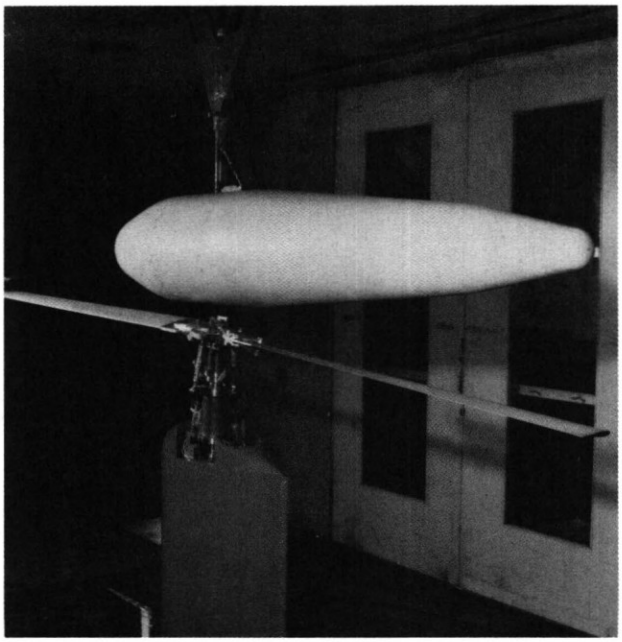

Figure 3. Rotor and body of revolution in the Ames 7- By 10-Foot Wind Tunnel.

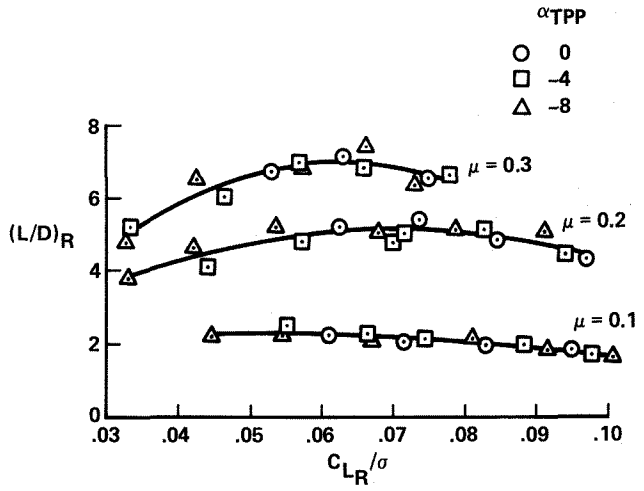

Figure 4. Isolated rotor performance.

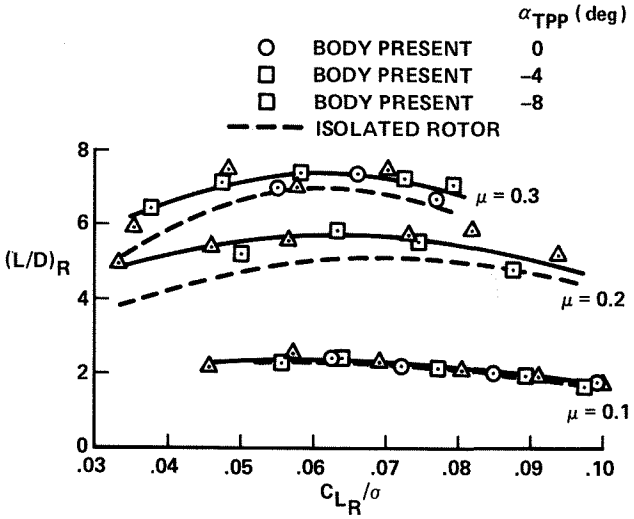

a) $\alpha_B = 0°$.

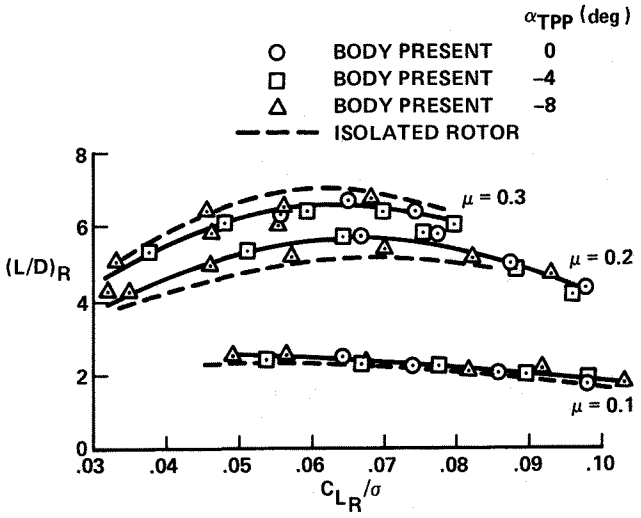

b) $\alpha_B = -4°$

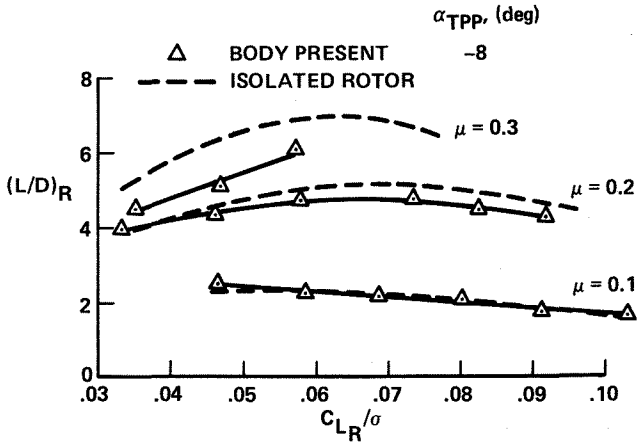

c) $\alpha_B = -8°$

Figure 5. Effect of body on rotor performance (baseline configuration).

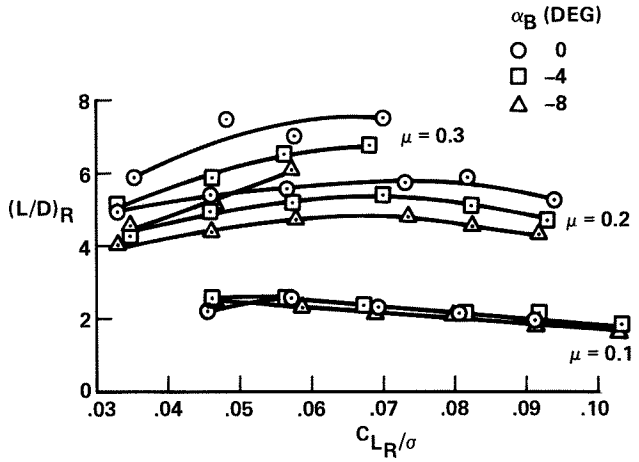

Figure 6. Effect of body angle of attack on rotor performance: α_{TPP} = -8°, baseline configuration.

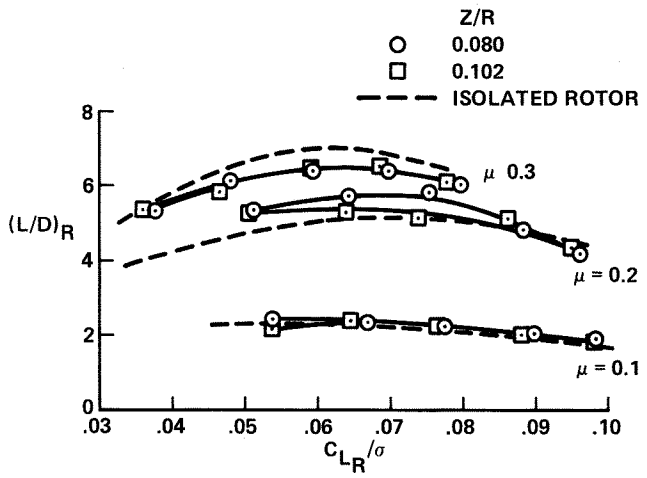

a) α_B = -4°, α_{TPP} = -4°

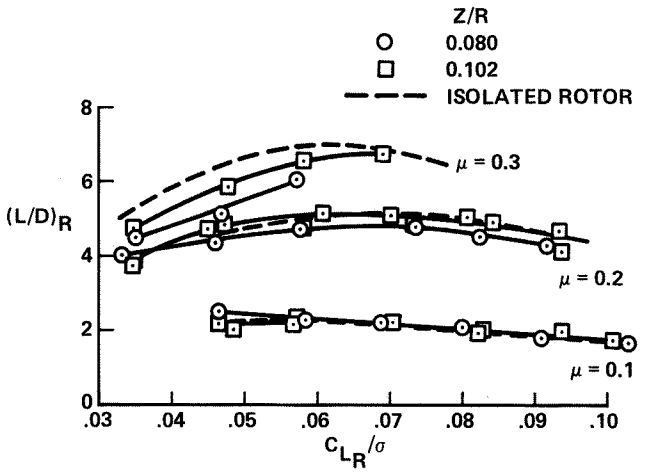

b) α_B = -8°, α_{TPP} = -8°

Figure 7. Effect of rotor/body separation on rotor performance.

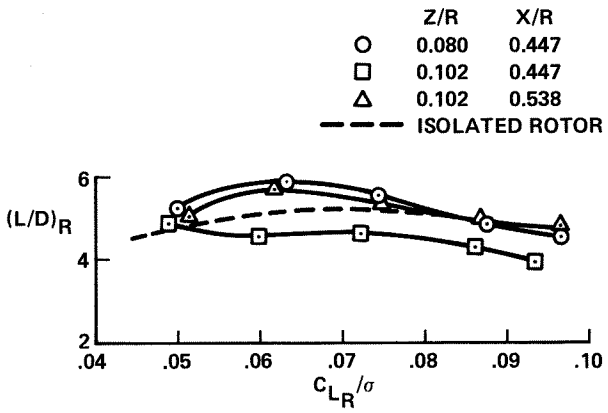

a) α_B = 0°, α_{TPP} = -4°, μ = 0.2

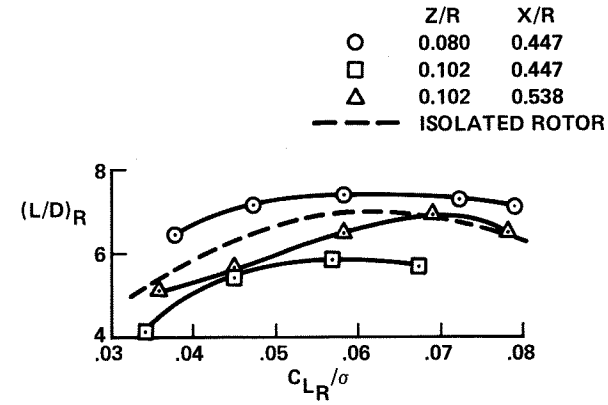

b) α_B = 0°, α_{TPP} = -4°, μ = 0.3

Figure 8. Effect of body position on rotor performance.

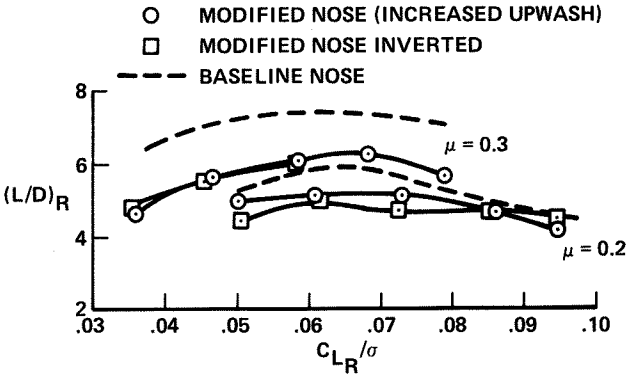

Figure 9. Effect of body nose configuration on rotor performance: α_B = 0°, α_{TPP} = -4°, baseline position.

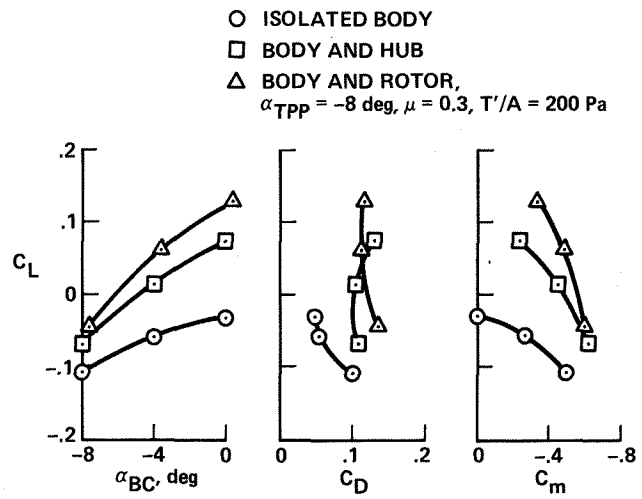

Figure 10. Effect of hub and rotor on body longitudinal characteristics: V = 61.7 m/sec, baseline configuration.

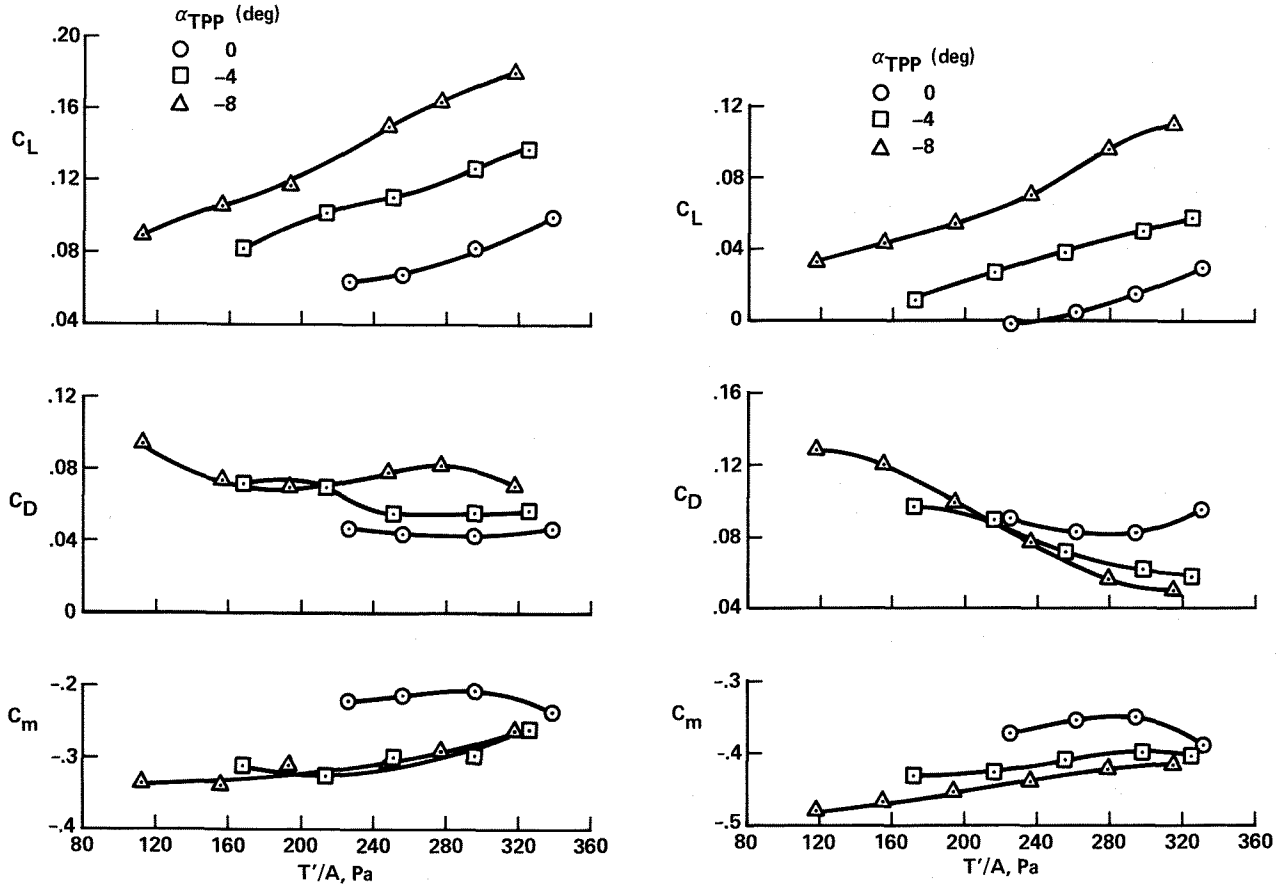

a) α_B = 0°, μ = 0.2, V = 41.2 m/sec

b) α_B = −4°, μ = 0.2, V = 41.2 m/sec.

Figure 11. Effect of rotor thrust on body longitudinal characteristics (baseline configuration).

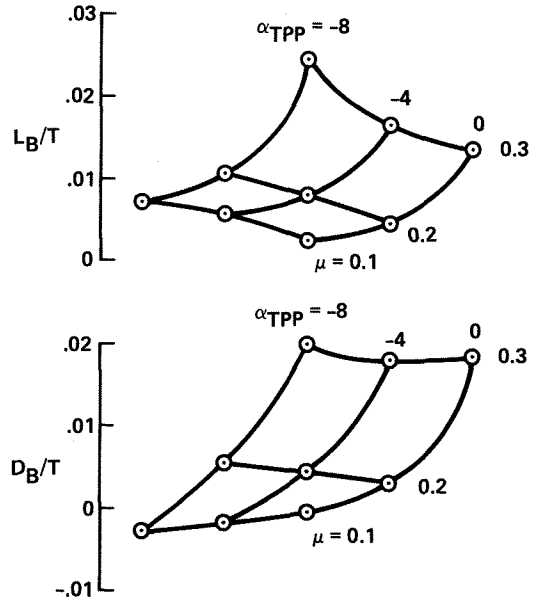

a) α_B = 0°, T'/A = 240 Pa

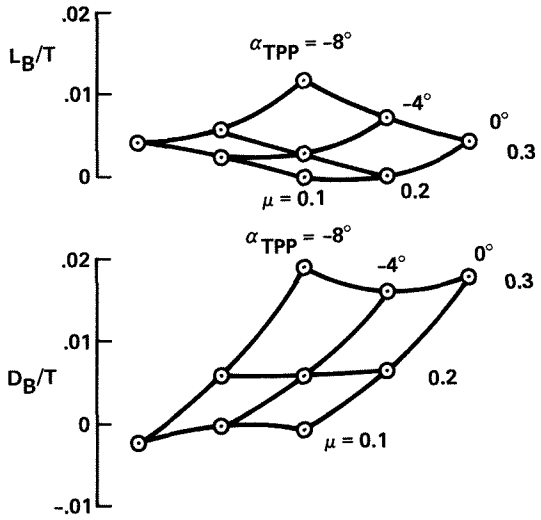

b) α_B = -4°, T'/A = 240 Pa

Figure 12. Effect of rotor tip-path-plane angle of attack on body lift and drag (baseline configuration).

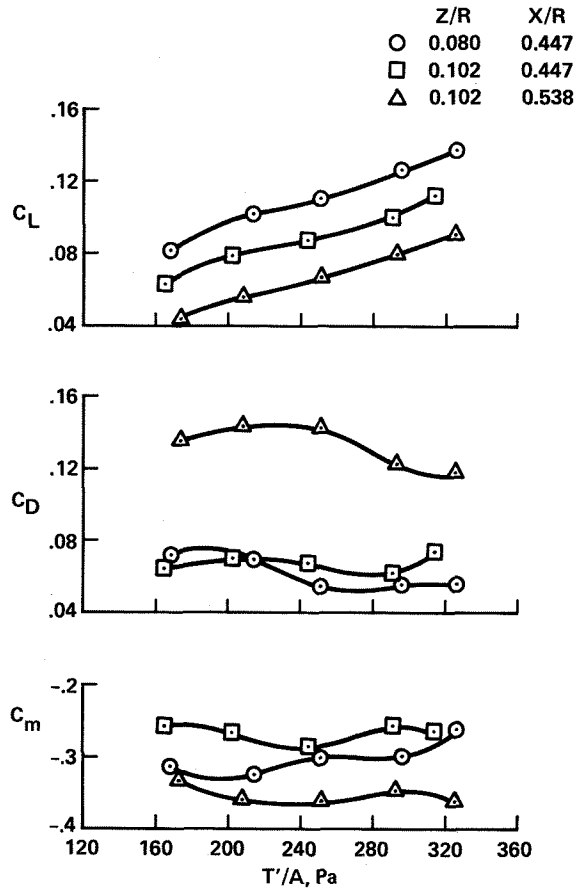

Figure 13. Effect of rotor position on body longitudinal characteristics: α_B = 0°, α_{TPP} = -4°, μ = 0.2, V = 41.2 m/sec.

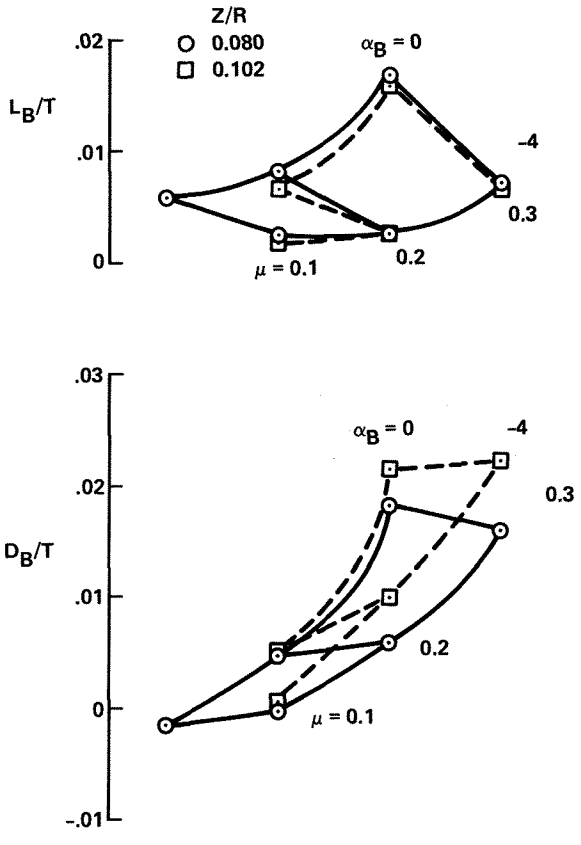

Figure 14. Effect of rotor/body separation on body lift and drag: T'/A = 240 Pa, α_{TPP} = -4°, X/R = 0.447.

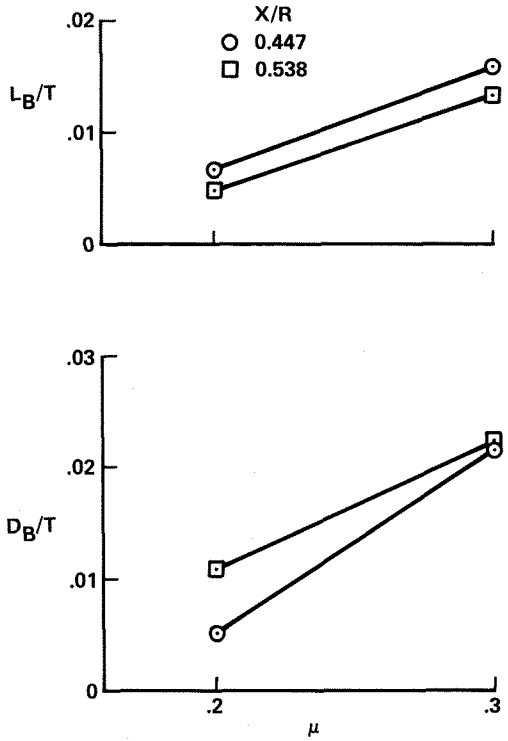

Figure 15. Effect of longitudinal position of rotor on body lift and drag: $\alpha_B = 0°$, $\alpha_{TPP} = -4°$, $T'/A = 240$ Pa, $Z/R = 0.102$.